Effect of Disorder on Ultrafast Exciton Dynamics Probed by Single Molecule Spectroscopy

Jordi Hernando,[1,2] Erik M. H. P. van Dijk,[1] Jacob P. Hoogenboom,[1] Juan-José García-López,[1] David N. Reinhoudt,[1] Mercedes Crego-Calama,[1] María F. García-Parajó,[1,3,4] and Niek F. van Hulst[1,4,5,*]

[1]*MESA+ Institute for Nanotechnology, University of Twente, 7500 AE Enschede, The Netherlands*
[2]*Departament de Química, Universitat Autònoma de Barcelona, 08193 Cerdanyola del Vallès, Spain*
[3]*Laboratory of NanoBioengineering, Barcelona Scientific Park (PCB), Josep Samitier 1-5, 08028 Barcelona, Spain*
[4]*ICREA—Institució Catalana de Recerca i Estudis Avançats, 08015 Barcelona, Spain*
[5]*ICFO—Institut de Ciències Fotòniques, 08860 Castelldefels, Spain*

(Received 23 February 2006; published 20 November 2006)

We present a single-molecule study unraveling the effect of static disorder on the vibrational-assisted ultrafast exciton dynamics in multichromophoric systems. For every single complex, we probe the initial exciton relaxation process by an ultrafast pump-probe approach and the coupling to vibrational modes by emission spectra, while fluorescence lifetime analysis measures the amount of static disorder. Exploiting the wide range of disorder found from complex to complex, we demonstrate that static disorder accelerates the dephasing and energy relaxation rate of the exciton.

DOI: 10.1103/PhysRevLett.97.216403 PACS numbers: 71.35.Aa, 32.50.+d, 78.47.+p

For many decades assemblies of coupled emitters have been studied intensively due to their intriguing properties of spectral narrowing [1] and enhancement of spontaneous emission rate (superradiance) [2]. This behavior stems from coherent excited state energy (exciton) delocalization over the aggregate [3,4]. The exploitation of exciton delocalization for a controlled transfer of energy in photonics and electronics devices as well as in novel schemes for quantum computation has sparked new interest in a wide variety of multichromophoric assemblies, such as photonic polymers [5], light harvesting complexes [6], and quantum dot arrays [7]. In practice, the performance of these systems depends on the extent of coherent exciton delocalization, a property varying in time and space due to static and dynamic disorder [8,9]. Understanding how these two parameters constrain the extent of collective excited states in multichromophoric assemblies is therefore a crucial step in the design of functional excitonically based molecular devices.

Static disorder in dye assemblies mainly arises from differences in the energy of the interacting chromophores. The initial exciton created upon absorption is then confined to a region smaller than the actual size of the complex [10]. Coupling of this state to molecular vibrations and bath phonon modes (dynamic disorder) leads to subsequent ultrafast dephasing and energy relaxation through the exciton band. As a consequence, the coherence size of the exciton is further reduced [11]. Therefore, the properties of the final thermalized exciton result from the action of both static and dynamic disorder. The combined effects of these parameters on exciton dynamics have been studied so far theoretically [12] and by means of bulk spectroscopy [13]. In bulk experiments, however, the interplay of static and dynamic disorder cannot be disentangled since the average over a wide range of energy differences from molecule to molecule is measured.

In this Letter we investigate the effect of static disorder on exciton dynamics in a multichromophoric system using a unique combination of several room-temperature single-molecule spectroscopy (SMS) techniques. The coherent delocalization length of the final thermalized exciton is probed using steady-state and fast SMS methods, thus unraveling the extent of static disorder in individual aggregates. The interplay between static disorder and exciton dynamics is then investigated by simultaneous measurement of the ultrafast relaxation process of the initial exciton state, which is carried out by means of a recently developed single-molecule pump-probe (SM2P) method [14,15]. Remarkably, we find that static disorder strongly determines exciton dynamics.

The assemblies investigated in this work are dimers and trimers of the tetraphenoxy-perylene diimide dye (PD) presenting a rigid head-to-tail structure with a parallel orientation of the transition dipole moments of the constituent PD units [16]. A strong dipolar interaction is calculated for adjacent PD chromophores, leading to coherent exciton delocalization [16]. Thin films of poly(methyl methacrylate) doped with PD monomers, dimers (DPD), and trimers (TPD) were studied by means of both SMS and SM2P. In SMS measurements [16], the time evolution of fluorescence intensity, lifetime, and spectrum was monitored for individual molecules excited with 280 fs pulses at $\lambda = 568$ nm (circularly polarized light), repetition rate of 8 MHz, and mean power density of 2.5 kW cm^{-2}. In SM2P experiments [14,15], molecules were excited at $\lambda = 580$ nm (circularly polarized, 1 MHz, 4 kW cm^{-2}) with two consecutive identical saturating pulses (FWHM = 280 fs) whose mutual delay ($\Delta\tau$) was continuously scanned from ~ -2 ps to $\sim +2$ ps while simultaneously acquiring the fluorescence intensity and lifetime.

SMS measurements reveal the occurrence of multilevel intensity trajectories for individual DPD and TPD assem-

blies, a situation stemming from sequential photodamage of the constituent chromophores in the complexes [16,17]. This behavior is shown in Fig. 1(a) for a single TPD molecule, whose high (level 3), intermediate (level 2), and low (level 1) fluorescence intensity levels arise from a trimer with three, two, and one intact PD units, respectively. Examination of the properties of these separate levels reveals the effect of dye coupling on the behavior of each assembly.

Figures 1(b) and 1(c) show both the fluorescence decays and spectra for a single TPD molecule. The fluorescence lifetime (τ_f) recovered by exponential fitting of the decays lowers with increasing number of interacting chromophores: $\tau_{f3} = 3.9$ ns, $\tau_{f2} = 4.9$ ns, and $\tau_{f1} = 6.5$ ns. We have previously shown that such decrease arises from the occurrence of superradiance [16], i.e., enhancement of the radiative rate of the assembly due to exciton delocalization over the coupled chromophores [3,4]. Indeed, the ratio between the τ_f values for the lowest and highest intensity levels directly yields in this case the degree of superradiance (L_S) of the system [16]. Exciton delocalization also accounts for the shift and changes in the relative intensity of vibronic bands observed for the spectral data in Fig. 1(c). This second result can be quantified by means of the Huang-Rhys factor (S), defined as the intensity ratio between the 1-0 ($\lambda \sim 660$) and 0-0 ($\lambda \sim 610$ nm) emission bands [18]. This factor provides a direct measure for the coupling of the excited state and a certain molecular vibration. For the spectra depicted in Fig. 1(c), $S_3 = 0.29$, $S_2 = 0.34$, and $S_1 = 0.50$. Thus, S lowers due to chromophore interaction, rendering a reduced contribution of vibronic bands and a narrowing of the spectrum for the intact assembly [4,18]. The delocalized nature of the exciton is responsible for this decreased coupling between the electronic state and the vibrational mode resolved in the trimer spectra.

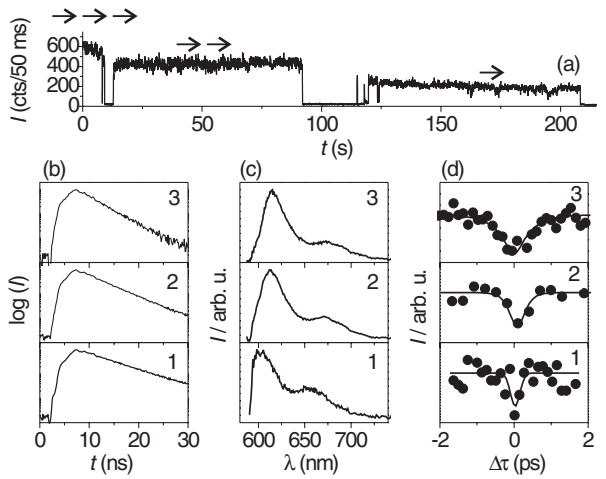

FIG. 1. (a) Fluorescence intensity (I) trace for a trimer. Arrows on top of the intensity trace schematically indicate the orientation of the transition dipole moments of the active PD units. Fluorescence decays (b) and spectra (c) for the levels 3 ($t =$ 0–10 s), 2 ($t =$ 10–90 s), and 1 ($t =$ 120–210 s) of trace (a). The 0-0 and 1-0 emission bands appear at $\lambda \sim 610$ nm and $\lambda \sim$ 660 nm, respectively, in (c). (d) SM2P dips for the levels 3, 2, and 1 of a trimer, showing a decrease in fluorescence intensity at $\Delta\tau = 0$ of 16% (3), 10% (2), and 16% (1). The solid lines are fits which recover the redistribution times.

Coupling between electronic and vibrational degrees of freedom also governs the ultrafast dynamics of excited states prior to their decay to the ground level. We use the recently developed SM2P method [14,15] to unravel this process for individual assemblies. Figure 1(d) displays the results obtained on a single trimer. For each intensity level a clear dip in fluorescence intensity at zero delay between the pump and probe pulses is observed, which is interpreted as follows. At $\Delta\tau = 0$ the emission is not increased due to the second probe pulse, since the first pump pulse already saturated the transition. For $\Delta\tau \neq 0$, however, coupling to phonons leads to dephasing and relaxation of the initially excited state prior to the arrival of the probe pulse. Consequently, the optical transition is no longer saturated and an increase of fluorescence does result from the second pulse [14,15]. The width of the dip therefore reports on the ultrafast dynamics of the initially excited state. The narrower the dip, the faster the energy relaxation driven by coupling to phonons, which has been attributed to an intramolecular energy redistribution process [15]. Since the energy of pump and probe pulses is equal and their spectral bandwidth relatively narrow ($\sim$90 cm^{-1}), our SM2P method is particularly sensitive to the onset of such energy redistribution.

The measured dips in Fig. 1(d) have been fit with a three level model, accounting for the pulse length, to derive characteristic redistribution times (τ_{er}) [15]. We obtain values of $\tau_{er} = 0.48$, 0.18, and 0.04 ps for levels 3, 2, and 1 of the particular trimer in Fig. 1, respectively. Clearly, the redistribution time increases due to chromophore interaction, suggesting a decrease in phonon coupling efficiency upon delocalization, consistent with the spectral data. However, it should be noted that SM2P experiments report on the interaction of the *initial* exciton to a manifold of phonon modes, while emission spectra reflect the coupling of the *final* thermalized exciton to a single, high energy vibrational mode.

The trends in τ_f, S, and τ_{er} shown in Fig. 1 for the different intensity levels of a single trimer were observed for all investigated DPD and TPD complexes. Yet, the extent of changes of τ_f, S, and τ_{er} with dye interaction was found to vary from molecule to molecule. Thus, broad distributions of L_S were retrieved from τ_f measurements on 55 DPD and 119 TPD assemblies [Fig. 2(a)], whose average values are 1.2 and 1.5, respectively. In case of linear assemblies with parallel interacting dipoles such as DPD and TPD, L_S provides a direct estimate of the exciton coherent delocalization length [8]. Therefore, the spread in L_S values and the deviation of the mean with respect to the ideal situation ($L_S = 2$ for TPD and $L_S = 2.9$ for TPD

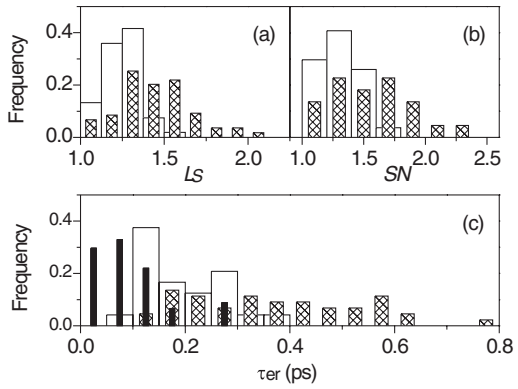

FIG. 2. (a) Distributions of the degree of superradiance (L_S) for 55 DPD (open) and 119 TPD (crossed) assemblies. For DPD, L_S is defined as τ_{f1}/τ_{f2} and for TPD, τ_{f1}/τ_{f3}. (b) Distributions of the degree of spectral narrowing (SN) for 27 DPD (open) and 22 TPD (crossed). SN is defined as S_1/S_2 for DPD and S_1/S_3 for TPD. (c) Histograms of the energy redistribution time (τ_{er}) for the highest intensity levels of 91 PD (black), 24 DPD (open), and 44 TPD (crossed) molecules.

[3,4]) evidence a reduction of the exciton coherence size due to disorder varying from molecule to molecule.

Figure 2(b) shows the ratios of the Huang-Rhys factor between the lowest and highest intensity levels of all investigated DPD and TPD assemblies. These S ratios report on the spectral narrowing (SN) due to a decreased vibronic coupling arising from exciton delocalization. Clearly, a significant spread in SN is also found, with average values of SN = 1.3 (DPD) and SN = 1.7 (TPD), again lower than expected in absence of disorder [SN = 2 (DPD) and 3 (TPD) [18]].

Figure 2(c) shows the ultrafast redistribution times for the highest intensity levels of all PD, DPD, and TPD molecules investigated. For PD monomers a relatively narrow distribution centered at low values of τ_{er} is observed ($\langle\tau_{er}\rangle = 0.094$ ps). In this case the spread in τ_{er} is attributed to slight molecular conformational differences induced by the nanoenvironment surrounding the molecule [14,15]. On the other hand, the distributions for DPD and TPD in Fig. 2(c) are broader and shifted to larger values of τ_{er} [$\langle\tau_{er}\rangle = 0.19$ (DPD) and 0.38 ps (TPD)]. This indicates that coherent exciton delocalization in the aggregates reduces coupling to phonons, thus slowing down the ultrafast excited state dynamics. Variation in exciton coherence size from molecule to molecule due to disorder therefore accounts for the additional broadening of the DPD and TPD histograms.

In the distributions plotted in Fig. 2, both L_S and SN are time-integrated values over the entire duration of the excited state relaxation of the system. As such, they report on the properties of the final thermalized exciton state. However, while L_S provides a direct estimate of the delocalization length of this state, SN is a measure for the coupling strength to the dominant molecular vibration at $\omega \sim 1245$ cm^{-1}. Noticeably, the correlation plot of L_S and SN in Fig. 3(a) shows a clear correspondence between these two quantities. Thus, a Pearson's correlation coefficient of 0.78 is found between L_S and SN for the whole set of data points plotted in Fig. 3(a), whose deviation from zero has a statistical significance better than 99%. Therefore, our data support that larger exciton delocalization yields lower coupling to vibrational modes, as theory predicts [3,4].

The correlation between L_S and SN can be modeled theoretically by means of a Holstein Hamiltonian [18–20]:

$$H = E_{0\text{-}0} + S\omega + \omega\sum_i b_i^\dagger b_i + \sum_{i\neq j} J_{ij}|i\rangle\langle j| - \omega S^{1/2}\sum_i (b_i^\dagger + b_i)|i\rangle\langle i|, \quad (1)$$

where $E_{0\text{-}0}$ is the electronic excitation energy of the monomer, $|i\rangle$ ($|j\rangle$) stands for the state of the aggregate in which dye i (j) carries the electronic excitation, and $b_i^\dagger$ (b_i) is the creation (annihilation) operator for the vibration on unit i. The fourth term in (1) accounts for the exciton interaction energy between dyes i and j with coupling strength J_{ij}, and the fifth term describes the coupling between the electronic states and a single vibrational mode ($H_{\text{ex-ph}}$). With respect to the monomer, the exciton-phonon interaction for a particular dye unit in the assembly, i.e., $\langle i|H_{\text{ex-ph}}|\Psi\rangle$, is weighted by its partial contribution to the overall exciton wave function Ψ. This results in a decrease of coupling to vibrations upon exciton delocalization, as experimentally inferred from our spectral and SM2P results.

To solve (1) for DPD and TPD, J_{ij} was computed assuming a dipole-dipole model ($J_{i,i+1} = -300$ cm^{-2} and $J_{i,i+2} = -37.5$ cm^{-1} [16]), while the frequency ($\omega = 1245$ cm^{-1}) and Huang-Rhys factor ($S = 0.47$) of the vibrational mode of interest were derived from the spectral data of 24 monomers. To account for static disorder, numerical simulations of (1) were run by randomly deriving $E_{0\text{-}0}$ from a Gaussian distribution with a mean value of $\nu = 16\,670$ cm^{-1} and a width of $\sigma_d = 320$ cm^{-1}, as deter-

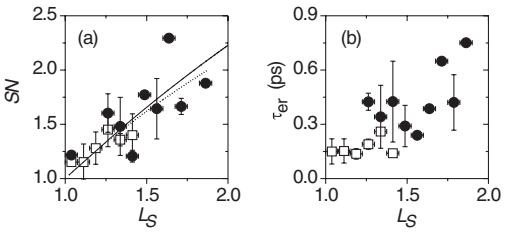

FIG. 3. (a) Spectral narrowing (SN) versus degree of superradiance (L_S) for DPD (squares) and TPD (circles). The mean SN ratios and their standard deviations are plotted for 27 DPD and 22 TPD assemblies after binning every 0.075 L_S units. Lines correspond to the theoretical calculations for DPD (dashed) and TPD (solid). (b) Redistribution time (τ_{er}) versus L_S for DPD (squares) and TPD (circles). The mean τ_{er} values and their standard deviations are plotted for 14 DPD and 22 TPD after binning every 0.075 L_S units.

mined from 24 monomers. The coefficients of the eigenfunctions of (1) derived in these calculations were then used to compute the optical properties of dimers and trimers [18]. The correspondence between L_S and SN obtained in this way reproduces remarkably well the experimental trend in Fig. 3(a). To uncover the cause of the spread in both L_S and SN for DPD and TPD, we also performed detailed simulations. We numerically solved (1) assuming either no energy disorder ($\sigma_d = 0$ cm^{-1}) or no coupling to phonons ($S = 0$), so that their effect on the optical properties of the assemblies could be analyzed separately. Moreover, the simulations with $\sigma_d = 0$ cm^{-1} were performed at different values of the Huang-Rhys factor, in order to account for the spread in S observed for individual PD molecules. The calculations show that both energy disorder and coupling to phonons determine the average values of L_S and SN. However, our simulations reveal the spread in these magnitudes results mainly from static disorder, i.e., $\sigma_d > 0$. Therefore, both the variations in L_S and SN measured for DPD and TPD uncover the full range of energy disorder in the system.

In contrast to L_S and SN, τ_{er} probes the evolution of the initial exciton. To investigate the relationship between τ_{er} and L_S we plotted these quantities against each other. The results are shown in Fig. 3(b). Remarkably, a clear correlation between τ_{er} and L_S is obtained. Indeed a Pearson's correlation coefficient of 0.77 with a statistical significance of 99% is retrieved for the whole set of data depicted in Fig. 3(b). Correlation between the unbinned single-molecule values of τ_{er} and L_S also occurred regardless of analyzing the dimer and trimer data sets together or separately, the statistical significance of the analysis being better than 95% in all cases. Note that this relationship is not obscured by the intrinsic spread in τ_{er} values expected for equally delocalized states, as inferred from the width of the PD distribution in Fig. 2(c). Therefore, our measurements prove a direct correspondence between τ_{er} and L_S: the slower the ultrafast exciton dynamics, the larger the degree of superradiance.

As indicated above, L_S measures the delocalization of the final thermalized exciton for DPD and TPD, whereas τ_{er} reports on the coherence size of the initial exciton set up by absorption. Consequently, Fig. 3(b) uncovers the occurrence of a clear correspondence between the delocalization coherence length of the initial and final exciton states. On the other hand, we have also shown that the spread in L_S maps the range of energy disorder in the system. Therefore, the correlation observed between τ_{er} and L_S in Fig. 3(b) ultimately reveals that static disorder strongly influences the rate of dephasing and energy redistribution of the initial exciton, an effect herein uncovered experimentally for the first time. Indeed, our results demonstrate that energy disorder accelerates the phonon-assisted relaxation process of the exciton.

In conclusion, we have investigated in this Letter the influence of static disorder on exciton dynamics in a system of coherently interacting chromophores by exploiting a combination of steady-state, fast, and ultrafast single-molecule techniques. We have experimentally demonstrated that larger energy disorder in a dye assembly leads to a reduction of the delocalization length in correspondence with theoretical predictions. Remarkably, we have also proven that disorder strongly governs the ultrafast relaxation of the initial coherent exciton state, leading to faster intraband dephasing and energy relaxation. Thus, experimental control and theoretical understanding of static energy disorder is of crucial importance for the design of molecular devices in photonics, light harvesting, and quantum entanglement.

This work has been supported by EC Program No. IHP-99 and the Spanish MCyT Program Ramón y Cajal (J. H.), the German VW-Stiftung (J. P. H.), and the Dutch Foundation FOM (E. M. H. P. v. D.).

*Electronic address: niek.vanhulst@icfo.es

[1] E. E. Jelley, Nature (London) **138**, 1009 (1936).
[2] R. H. Dicke, Phys. Rev. **93**, 99 (1954).
[3] A. S. Davydov, in *Theory of Molecular Excitons* (Plenum, New York, 1971).
[4] M. Kasha, H. R. Rawls, and M. Ashaf El-Bayoumi, Pure Appl. Chem. **11**, 371 (1965).
[5] A. Kohler *et al.*, Nature (London) **392**, 903 (1998).
[6] G. Trinkunas *et al.*, Phys. Rev. Lett. **86**, 4167 (2001).
[7] L. Quiroga and N. F. Johnson, Phys. Rev. Lett. **83**, 2270 (1999).
[8] T. Meier *et al.*, J. Chem. Phys. **107**, 3876 (1997); Y. Zhao *et al.*, J. Phys. Chem. B **103**, 3954 (1999).
[9] M. Bednarz, V. A. Malyshev, and J. Knoester, Phys. Rev. Lett. **91**, 217401 (2003).
[10] H. Fidder, J. Terpstra, and D. A. Wiersma, J. Chem. Phys. **94**, 6895 (1991).
[11] F. C. Spano, J. R. Kuklinski, and S. Mukamel, Phys. Rev. Lett. **65**, 211 (1990).
[12] V. Chernyak and S. Mukamel, J. Chem. Phys. **105**, 4565 (1996); D. J. Heijs, V. A. Malyshev, and J. Knoester, Phys. Rev. Lett. **95**, 177402 (2005).
[13] K. Ohta, M. Yang, and G. R. Fleming, J. Chem. Phys. **115**, 7609 (2001); S. S. Lampoura *et al.*, J. Phys. Chem. B **104**, 12 072 (2000).
[14] E. M. H. P. van Dijk *et al.*, Phys. Rev. Lett. **94**, 078302 (2005).
[15] E. M. H. P. van Dijk *et al.*, J. Chem. Phys. **123**, 064703 (2005).
[16] J. Hernando *et al.*, Phys. Rev. Lett. **93**, 236404 (2004).
[17] M. Lippitz *et al.*, Phys. Rev. Lett. **92**, 103001 (2004).
[18] F. C. Spano, J. Chem. Phys. **116**, 5877 (2002).
[19] M. Hoffmann and Z. G. Soos, Phys. Rev. B **66**, 024305 (2002).
[20] See EPAPS Document No. E-PRLTAO-97-023648 for a detailed supporting information on the theoretical model used to investigate the radiative properties of dimers and trimers of perylenediimide. For more information on EPAPS, see http://www.aip.org/pubservs/epaps.html.